Rapid toxin sequestration impacts poison frog physiology

Lauren A. O'Connell[1,2]*, LS50: Integrated Science Laboratory Course[2], Jeremy D. O'Connell[3], Joao A. Paulo[3], Sunia A. Trauger[4], Steven P. Gygi[3], and Andrew W. Murray[2,5]

1 Department of Biology, Stanford University, Stanford, CA 94305, USA

2 LS50b: Integrated Science Laboratory Course, Harvard University, Cambridge, MA 02138, USA

3 Department of Cell Biology, Harvard Medical School, Boston, MA 02115, USA

4 Harvard Center for Mass Spectrometry, Harvard University, Cambridge, MA 02138, USA

5 Department of Molecular and Cellular Biology, Harvard University, Cambridge, MA 02138, USA

Key words: alkaloids, proteomics, saxiphilin, complement system, cytochrome P450s

*To whom correspondence should be addressed:
Lauren A. O'Connell
Department of Biology
Stanford University
371 Jane Stanford Way
Stanford, CA 94305
loconnel@stanford.edu

Abstract

Poison frogs sequester their chemical defenses from their diet of leaf litter arthropods for defense against predation. Little is known about poison frog physiological adaptations that confer this unusual ability to bioaccumulate dietary alkaloids from the intestines to skin glands for storage. We conducted an alkaloid-feeding experiment with the Diablito poison frog (*Oophaga sylvatica*) to determine how quickly toxins are accumulated and how toxins impact frog physiology using quantitative proteomics. Diablito frogs were able to rapidly accumulate the alkaloid decahydroquinoline to the skin storage glands within four days of dietary exposure, with decahydroquinoline also detected in the intestines and liver. Alkaloid exposure impacted tissue physiology, with protein abundance shifting in the intestines, liver, and skin. Many proteins that increased in abundance with toxin accumulation are plasma glycoproteins, including components of the complement system and the toxin-binding protein saxiphilin. Other protein classes that change in abundance with toxin accumulation are membrane proteins involved in small molecule transport and metabolism, including ABC transporters, solute carrier proteins, and cytochrome P450s. Overall, this work shows that poison frogs can rapidly accumulate alkaloid toxins, which alter carrier protein abundance, initiate an immune response, and alter small molecule transport and metabolism dynamics across tissues. More broadly, this study suggests that acute changes in diet may quickly change the chemical arsenal and physiology of poison frogs, which may have important consequences in their defense against predation.

Introduction

Many organisms can acquire chemical defenses from external sources. These acquired chemical defenses are sometimes diet-derived and many examples can be found in invertebrates (Opitz and Müller, 2009) and less commonly in vertebrates (Opitz and Müller, 2009; Savitzky et al., 2012). Poison frogs sequester lipophilic alkaloids from arthropod prey (Saporito et al., 2009), which requires specialized physiology for bioaccumulation and toxin resistance (Santos et al., 2016). The bioaccumulation of alkaloids requires coordination between several tissue systems, from absorption in the gut, transport between tissues, and storage in skin granular glands. Although sequestering defensive chemicals involves a well-studied ecological and evolutionary relationship between arthropod prey and frog predators (Darst et al., 2005; Saporito et al., 2011), how poison frogs sequester alkaloids is unknown.

The chemical defenses of poison frogs mainly consist of small molecules, including lipophilic alkaloids. Over 800 alkaloids have been characterized in poisonous amphibians (Daly et al., 2005), highlighting species diversity in chemical defense, particularly in South American dendrobatid poison frogs (Saporito et al., 2011). The ability to sequester alkaloids evolved several times in dendrobatids and coincides with a dietary specialization on ants and mites (Darst et al., 2005; Santos et al., 2003). The dietary hypothesis of poison frog toxicity arose when several studies noted that poison frogs reared in captivity lacked alkaloids (Daly et al., 1994a). Several pioneering studies utilized this biological feature to examine alkaloid uptake and metabolism (Daly et al., 1994b; Hantak et al., 2013), although the rate of alkaloid uptake is unclear. Research over several decades has focused on alkaloid characterization (Saporito et al., 2011), but how poison frogs take up and store toxins remains largely unexplored.

Although alkaloids are lipophilic, these small molecules do not seem to simply perfuse passively throughout the organism. Evidence for an uptake system in poison frogs comes from alkaloid quantification in various tissues, including the liver, muscles, and oocytes (Prates et al.,

2011; Stynoski et al., 2014), although alkaloids are most abundant in the skin where they are stored in granular glands (Neuwirth et al., 1979). Moreover, the vertebrate intestinal lining is well-equipped to prevent passive absorption of toxic substances using a series of membrane transporters. These transport proteins interact with dietary compounds for movement either back into the lumen for excretion or into the blood for circulation (Zhang and Benet, 2001). Absorbed lipophilic molecules are then transported through the blood circulation bound to carrier proteins produced by the liver. The molecular physiology of alkaloid bioaccumulation, metabolism, and transport between each of these poison frog tissue systems is unknown.

We conducted an experiment to determine how alkaloid sequestration impacts frog physiology and tested the general hypothesis that alkaloid bioaccumulation alters the abundance of proteins involved in small molecule transport and metabolism. We used the Diablito frog (*Oophaga sylvatica*) to address this question, which complements our previous studies examining the chemical ecology of this species (Caty et al., 2019; McGugan et al., 2016; Roland et al., 2016). Frogs were fed the alkaloid decahydroquinoline (DHQ), a commercially available alkaloid they naturally sequester in the wild (Caty et al., 2019), for various amounts of time and we examined how alkaloid sequestration influences frog physiology using quantitative proteomics. Our experiments show that poison frogs sequester alkaloids within four days of exposure, shifting protein abundance across tissues, including plasma glycoproteins and cytochrome P450s.

Materials and Methods

Animals

Adult Diablito frogs (*Oophaga sylvatica*, N=12) were purchased from Indoor Ecosystems (Whitehouse, OH, USA) and housed for three months prior to the experiment. Frogs were housed individually on a 12:12 hour photoperiod, immediately preceded and followed by a 10 min period of dim incandescent lights to simulate dawn and dusk. Frogs were misted with water three times daily and fed four times per week with fruit flies dusted with a vitamin supplement. The Institutional

Animal Care and Use Committee of Harvard University approved all procedures (Protocols 15-02-233 and 15-07-247).

Decahydroquinoline feeding experiment

Frogs were randomly assigned to one of four groups. The three experimental groups (N=3 per group) received fruit flies dusted with a 1% decahydroquinoline (DHQ; Sigma-Aldrich, St. Louis, MO, USA) in a vitamin mix (Dendrocare vitamin/mineral powder, Black Jungle, Turners Falls, MA, USA) for either 1, 4, or 18 days (Figure 1A). DHQ-like alkaloids are sequestered by *O. sylvatica* in the wild (Caty et al., 2019) and represent an ecologically relevant treatment. Control frogs (N=3) received flies dusted with vitamin mix without DHQ. For the 1-day group, frogs received toxin-dusted flies in the morning, and then were sacrificed the following day after receiving another dose of flies that morning (a total of 2 feedings in 36 hours). For the 4-day group, frogs were fed toxic flies on Monday, Tuesday, Thursday, and Friday mornings and were sacrificed Friday afternoon. For the 18-day group, frogs were fed toxic flies 4 days per week for 3 weeks for a total of 12 feedings. Roughly 15-25 flies (average = 18) flies were given to the frogs at each feeding session and the number of flies remaining the next morning were recorded. The average number of total alkaloid-dusted flies eaten by each group during the duration of the experiment were 14.3 for 1-day, 52.3 for 4-day, and 149.7 for 18-day. On the afternoon of the last day, the frogs were anesthetized by applying 20% benzocaine gel to the ventral side and then euthanized by decapitation. Dorsal skin, liver, and intestines were dissected, flash frozen in liquid nitrogen and stored at -80°C for later processing.

To isolate proteins and alkaloids from the same tissue samples, flash frozen tissues were removed from -80°C and immediately crushed to a powder in liquid nitrogen using a mortar and pestle. Tissue powder was then resuspended in a lysis buffer from the Mammalian Cell Lysis kit containing a protease inhibitor cocktail (Sigma-Aldrich). Samples were incubated in a lysis buffer at 4°C for 15 min rotating and then centrifuged for 20,000 x g for 10 min at 4°C to pellet cell debris;

the supernatant was transferred to a chilled microcentrifuge tube. Protein concentration was determined using 2 µl of lysate in a Bicinchoninic Acid (BCA) Assay according to manufacturer's instructions (Thermo Scientific, Waltham, MA, USA). To standardize the amount of input material in downstream assays, lysate containing 300 µg of protein from each tissue type was transferred to a chilled microfuge tube for protein and alkaloid (DHQ) extraction. A chloroform-methanol extraction was used to separate the DHQ and proteins from the same tissue lysate sample. Briefly, 400 µl 100% methanol was added to each sample and then each sample was vortexed. Then 100 µl chloroform was added to each sample, which was immediately vortexed. To precipitate the protein, 200 µl nuclease-free water was added to each sample. After vortexing, samples were centrifuged at 21,000 x g for 3 min at room temperature, resulting in a protein disk at the interface of the aqueous methanol top layer and the organic chloroform bottom layer. A previous pilot experiment showed roughly 90% of DHQ spiked into a protein lysate sample separated into the chloroform layer. Therefore, the methanol layer was removed and the chloroform layer was isolated into a glass vial and stored at -20°C for later quantification of DHQ. The remaining protein pellet was rinsed twice with 1 mL methanol and then stored at -80°C for further processing.

Quantification of DHQ

Liquid chromatography / mass spectrometry (LC/MS) quantification of DHQ was performed on a Bruker maXis Impact Q-TOF system (Billerica, MA) with an Agilent 1290 LC (Palo Alto, CA). A reversed-phase LC gradient method was used using a Dikma C8, 3 µm particle size, 2.1 x 100 mm column (Dikma, Lake Forest, CA). Mobile phase A was composed of water with 0.1% formic acid and mobile phase B was composed of acetonitrile with 0.1% formic acid. The flow rate was 0.3 mL/min. The gradient began with 0% B for two min then increased linearly to 100% B at 8 min and was held until 10 min. The solvent composition was then returned to starting aqueous conditions to re-equilibrate the column for the next injection. The mass spectrometer

was tuned for standard mass range analysis and data were continually acquired in the range m/z 50-3000; each run was recalibrated for the m/z scale using a post-run injection of a sodium formate solution. Electrospray positive mode ionization was used with a source drying gas of 10 L/min at 200°C, nebulizer at 30 psi, and capillary set at 4000 V with an endplate offset of 500 V. For the Agilent Q-TOF, the Ion Funnel electrospray positive mode source used drying gas of 14 L/min at 200°C with nebulizer at 35 psi, a sheath gas flow of 11 L/min at 350°C, capillary set at 3500 V, nozzle voltage of 1000 V, and Fragmentor set at 175 V. Collision energies were set at 15 and 30 eV and data were continually acquired in the range m/z 50−1700 using a reference lock mass. A DHQ standard was run along with the experimental samples to identify the correct peak and the structure was confirmed by its fragmentation pattern using tandem mass spectrometry (Figure S1).

Quantitative proteomics

Protein disks were thawed and resuspended in 10 µl acetonitrile with gentle agitation to break up the disk, followed by the addition of 90ul 8M urea in 100mM EPPS pH 8.5 with another round of gentle vortexing. Samples were spun down at 13,000g for 30s, and sonicated in a water bath for 20 minutes at room temperature to complete resuspension. Proteins disulfide bonds were reduced with 5 mM tris-(2-carboxyethyl)-phosphine (TCEP), at room temperature for 25 min, and alkylated with 10 mM iodoacetamide at room temperature for 30 min in the dark. Excess iodoacetamide was quenched with 15 mM dithiothreitol at room temperature for 15 min in the dark. Then a methanol-chloroform precipitation was performed again as described above. Protein disks were resuspended in 10ul of 8M urea, 200mM EPPS pH 8.5 with gentle vortexing followed by the addition of 90ul 200mM EPPS pH 8.5 to reach 100 µl and dilute to 0.8M urea. Proteins were then digested at room temperature with gentle agitation for 12 hrs with LysC protease at a 100:1 protein-to-protease ratio. Then, trypsin was added at a 100:1 protein-to-protease ratio and the reaction temperature raised to 37°C for 6hrs. Digests were spun at 10,000 g for 10 min and

the supernatant transferred to a new tube. Peptide concentrations were measured using the Quantitative Colorimetric Peptide assay kit (Thermo Scientific) according to the manufacturer's instructions. Following quantification, 50 µg of peptides from each sample were labelled with 5 µl of Tandem Mass Tag 10-plex (TMT, Thermo Scientific) reagent (0.02mg/µl) in 200mM EPPS pH8.5 at 30% acetonitrile (v/v) for 1 hour before quenching the reaction with 10 µl of 5% hydroxylamine. A pool of each time 0 sample was labelled collectively to create a bridge in an additional channel.

The TMT-labelled samples from each tissue from a given collection were then pooled in equimolar ratios, as verified by an MS2-only ratio check of an aliquot. The pooled sample was vacuum centrifuged to near dryness before resuspension in bicarbonate buffer, and separation by basic pH RP HPLC on an Agilent 1100 pump equipped with a degasser and a photodiode array (PDA) detector measuring at 220 and 280 nm wavelengths (Thermo Fisher Scientific - Waltham, MA). Peptides were subjected to a 50 min linear gradient from 8% to 80% acetonitrile in 10mM ammonium bicarbonate pH 8 at a flow rate of 0.6 mL/min over an Agilent 300Extend C18 column for 75 minutes (3.5 µm particles, 4.6 mm ID and 250 mm in length) to produce 96 equal volume fractions. The fractions were re-pooled down to 24 fractions, and vacuum centrifuged to reduce volume. The pooled fractions were acidified and then desalted via StageTip, vacuum centrifuged to near dryness, and reconstituted in 5% acetonitrile, 5% formic acid for injection into an Orbitrap Fusion Lumos.

Twelve fractions per analyzed following 3-hr gradient separations using a 4-40% isocratic gradient using a TOP10 method, where each FTMS1 scan was used to select up to 10 MS2 precursors for CID-MS2 followed by measurement in the ion trap. Each MS2 was used to select precursors (SPS ions) for the MS3 scan which measured reporter ion abundance for the 10 samples simultaneously (McAlister et al., 2014). Instrument parameter settings included an FTMS1 resolution of 120,000, ITMS2 isolation window of 0.4 m/z,120 ms ITMS2 max ion time,

ITMS2 AGC set to 2E4, ITMS2 CID energy of 35%, SPS ion count allowing up to 10 precursors, FTMS3 isolation window of 1.2 m/z, 150 ms FTMS3 max ion time, FTMS3 AGC set to 1.5E5, and FTMS3 resolution of 50,000.

Samples were searched with the Sequest algorithm (Ver. 28) against a custom *O. sylvatica* proteome database that was generated from transcriptome data (Caty et al., 2019) which was concatenated with their reversed sequences as decoys for FDR determination. Common contaminant sequences were similarly included. For searches we restricted the precursor ion tolerance to 50 ppm, and set the product ion tolerance window to 0.9 m/z, allowed up to two missed cleavages, included static medication of lysine residues and peptide N-termini with TMT tags (+229.163 Da), static carbamidomethylation of cysteine residues (+57.021 Da), and variable oxidation of methionine residues (+15.995 Da). The search results were combined and filtered to a 1% FDR at the peptide and protein levels using linear discriminant analysis and the target-decoy strategy (Elias and Gygi, 2010; Huttlin et al., 2010). MS3 spectra were processed as signal-to-noise ratios for each reporter ion based on noise levels within a 25 Th window. Proteins quantitation was the result of summing reporter ion intensities across all matching PSMs. PSMs with isolation specificity below 0.7, MS3 spectra with more than eight TMT reporter ion channels missing, or MS3 spectra with a TMT reporter ion summed signal to noise ratio that is less than 200 were removed before analysis. Overall, several thousand proteins were detected in each tissue type (5328 in the intestines, 5837 in the liver, and 5987 in the skin).

Data analysis

All statistics and figures were generated in R Studio (version 1.1.442) running R (version 3.5.2). For DHQ abundance, the integrated area under the peak from the ion chromatograph was used for sample quantification compared to the standard and values are presented in arbitrary units. We used the glmmTMB R package (Brooks et al., 2017) to run a generalized linear mixed model with a zero-inflated negative binomial distribution to test for significant differences in DHQ

quantity between groups and tissue type as main effects. Frog identity was included as a random effect to account for the sampling of three tissues (gut, liver, and skin) for each frog. We then followed the model with the Anova.glmmTMB function for reported statistical values. Boxplots were generated with the ggplot function in the ggplot2 package in R (version 3.3.0 (Wickham, 2009)).

For the proteomics data, protein contigs with fewer than two peptides were removed from the analysis, leaving 3715 in the intestines (69.7%), 3789 in the liver (64.9%), 3755 in the skin (62.7%). We combined the day 4 and day 18 animals with DHQ in all tissues in our proteomics analysis, totalling N=6 in the “toxic” group and N=3 in the “non-toxic” or control group. Day 1 was not included as we did not detect any DHQ in those samples and tandem mass tags for labeling was, at the time, limited to 10 tags. We used the eBayes() function in the R limma package (Ritchie et al., 2015) (version 3.36.5) to determine significant differences between groups in each tissue (D’Angelo et al., 2017). Tissues were analysed separately as they were TMT-labeled and run separately on the mass spectrometer. We considered protein contigs significantly different if they had a moderated p-value (adjusted for multiple testing) of $p < 0.05$ and a log fold change greater than 1. Volcano plots illustrating these cut-offs were generated with the EnhancedVolcano package (version 1.4.0, (Blighe et al., 2019)). Heatmaps for each tissue were generated with the heatmap.2 function of the gplots package (version 3.0.3). Gene ontology enrichment analyses were performed with the R package topGO (version 2.34.0; (Rahnenfuhrer, 2019)) with significance set at $p < 0.05$. Boxplots were generated with the ggplot function in the ggplot2 package in R (version 3.3.0, (Wickham, 2009)).

Results and Discussion

Poison frogs rapidly sequester toxins

We fed decahydroquinoline (DHQ) or vehicle control to captive-bred non-toxic Diablito (*Oophaga sylvatica*) poison frogs for 1, 4 or 18 days (Figure 1A) and quantified DHQ abundance across multiple tissues (Figure 1B). Although DHQ was not detectable one day after exposure, DHQ levels increased after 4 and 18 days in all tissues (Figure 1c). There was a significant effect of both Group (X^2(1)=16.387, p=5.163x10^{-5}) and Tissue (X^2(2)=10.331, p=0.001). Uptake within 4 days is faster than previous studies that documented skin alkaloid uptake after 3 months in bufonids (Hantak et al., 2013) and in 2-6 weeks in other dendrobatid species (Daly et al., 2003). We did not detect DHQ after 1 day, suggesting either DHQ did not reach the intestines by that time or abundance was below the limit of detection. Rapid uptake in dietary alkaloid toxins has important ecological implications, as acute shifts in arthropod diet could quickly contribute to the poison frog chemical repertoire and alter palatability to predators.

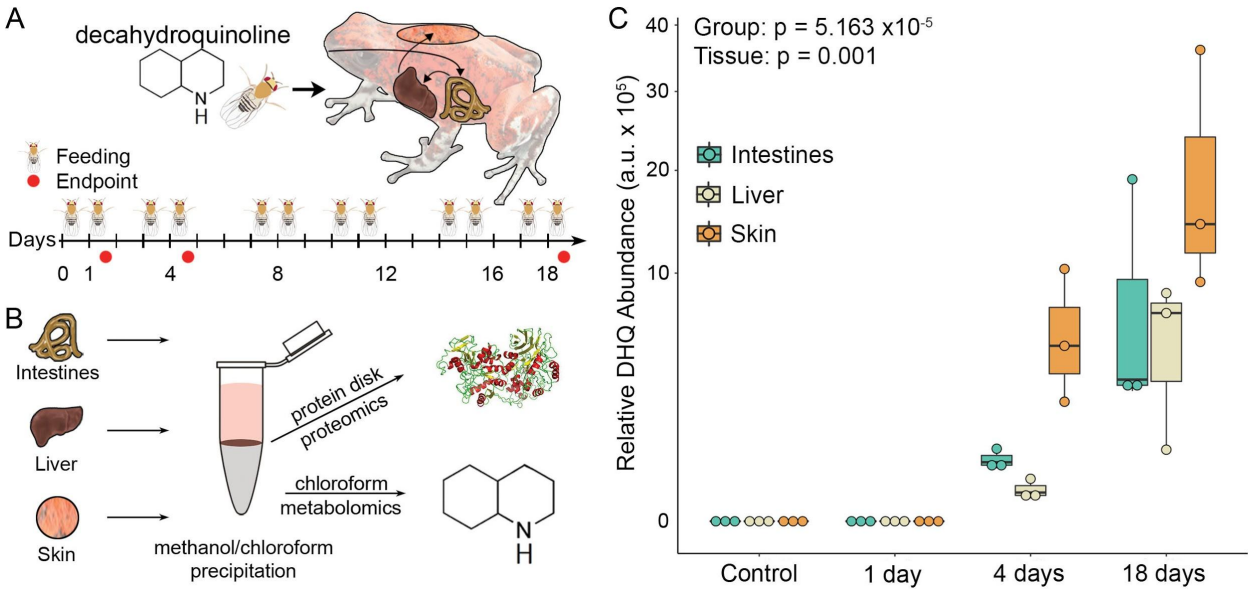

Figure 1. Rapid uptake of decahydroquinoline (DHQ). (A) Frogs were fed DHQ-dusted flies for various amounts of time to determine rate of toxin bioaccumulation. The number of times that frogs were fed with toxic flies and the endpoints are shown on the timeline. **(B)** Tissues were dissected and both protein and DHQ were isolated using methanol/chloroform precipitation. **(C)** Boxplots show DHQ abundance (y-axis, log scale) in the intestines (light green), liver (cream),

and skin (light orange) increase over time (N=3 frogs per group), with the first detectable amounts in all three tissues in 4 days. Results from the generalized linear mixed model are at the top left.

Decahydroquinoline exposure induces proteome shifts across tissues

As poison frogs rapidly uptake toxins, we then asked how frog physiology changes during DHQ uptake by examining protein abundance differences between control frogs and chemically defended frogs using quantitative proteomics (Figure 2, Supplementary Excel File, Figures S2-S4). Protein contigs in each tissue significantly varied with toxicity, including 276 in the intestines, 185 in the liver, and 278 in the skin. Across all tissues, there was significant gene ontology enrichment in four biological processes (Supplementary Excel File): negative regulation of endopeptidase activity, complement activation, inflammatory response, and oxidation-reduction processes. Plasma glycoproteins were increased in toxic frogs across all tissues (Figure 2A). Saxiphilin, an amphibian transferrin-like protein that binds the lethal alkaloid saxitoxin (Mahar et al., 1991; Yen et al., 2019), increased in abundance in the intestines and skin of toxic frogs (Table 1). We have previously shown that saxiphilin is more abundant in the plasma of non-toxic frogs and that saxiphilin may bind DHQ using thermal shift assays (Caty et al., 2019). Together, these data support the hypothesis that saxiphilin may carry alkaloid toxins in poison frogs through the circulation for deposition into the skin.

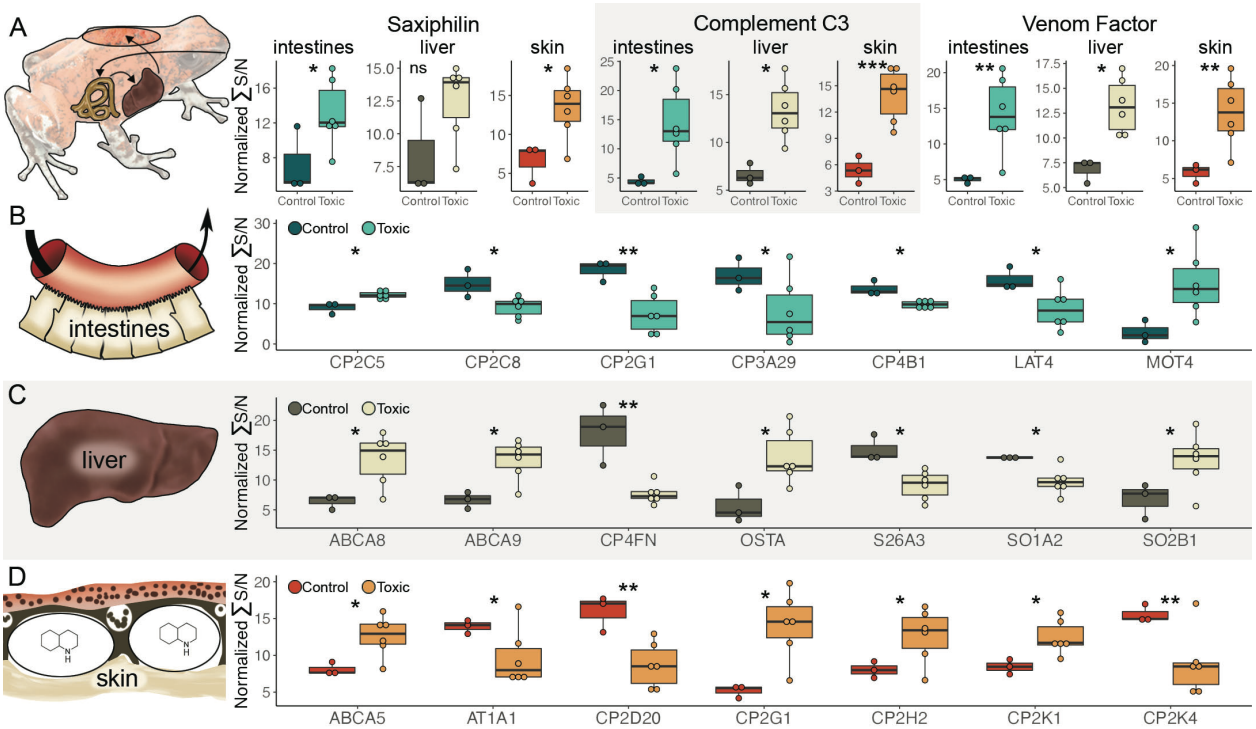

Figure 2. Proteomic changes with toxin bioaccumulation in the Diablito poison frog. (A) Some plasma glycoproteins were upregulated with toxicity across tissues, including saxiphilin, complement C3, and a venom factor. Y-axis shows the normalized sum of the signal to noise ratio. There were also many tissue-specific membrane protein abundance changes in the **(B)** intestines, **(C)** liver, and **(D)** skin that include small molecule transport and metabolism. See Table 1 for detailed statistics (* $p<0.05$, ** $p\leq0.005$, *** $p\leq0.0005$). Abbreviations: ABCA5, ATP Binding Cassette Subfamily A Member 5; ABCA8, ATP Binding Cassette Subfamily A Member 8; ABCA9, ATP Binding Cassette Subfamily A Member 9; AT1A1, ATPase Na+/K+ Transporting Subunit Alpha 1; CP2C5, Cytochrome P450 2C5; CP2C8, Cytochrome P450 2C8; CP2D20, Cytochrome P450 Family 2 Subfamily D Member 20; CP2G1, Cytochrome P450 2G1; CP2H2, Cytochrome P450 Family 2 Subfamily H Member 2; CP2K1, Cytochrome P450 Family 2 Subfamily K Member 1; CP2K4, Cytochrome P450 Family 2 Subfamily K Member 4; CP3A29, Cytochrome P450 3A29; CP4B1, Cytochrome 4B1; CP4FN, Cytochrome P450 Family 4 Subfamily F Member 22; LAT4, L-Type Amino Acid Transporter 4; MOT4, Monocarboxylate Transporter 4; OSTA, Solute Carrier Organic Anion Exchanger Family Member 26A3; Solute Carrier Family 51 Subunit Alpha; SO1A2, Solute Carrier Organic Anion Transporter Family Member 1A2; SO2B1, Solute Carrier Organic Anion Transporter Family Member 2B1.

Tissue	**Protein**	**LogFC**	t_{mod}	p_{mod}
Intestines	Saxiphilin (SAX)	2.03	2.53	0.030
	Complement C3 (CO3)	3.16	3.34	0.008
	Venom Factor (VCO3)	2.85	3.96	0.003
	Cytochrome P450 2C5 (CP2C5)	1.06	3.27	0.008
	Cytochrome P450 2C8 (CP2C8)	-1.45	-2.98	0.014

	Cytochrome P450 2G1 (CP2G1)	-3.00	-4.49	0.001
	Cytochrome P450 3A29 (CP3A29)	-2.49	-2.45	0.035
	Cytochrome P450 4B1 (CP4B1)	-1.01	-3.07	0.012
	Large Neutral Amino Acid Transporter Small Subunit 4 (LAT4/SO43A2)	-1.98	-3.14	0.011
	Monocarboxylate Transporter 4(MOT4/SO16A3)	3.43	2.66	0.024
Liver	Saxiphilin (SAX)	0.91	1.52	0.159
	Complement C3 (CO3)	1.61	2.98	0.014
	Venom Factor (VCO3)	1.51	3.11	0.011
	ATP Binding Cassette Subfamily A Member 8 (ABCA8)	1.85	2.48	0.032
	ATP Binding Cassette Subfamily A Member 9 (ABCA9)	1.72	2.77	0.019
	Cytochrome P450 4F22 (CP4FN)	-2.55	-4.82	0.0007
	Organic Solute Transporter Subunit Alpha (OSTA)	2.15	2.86	0.017
	Solute Carrier Organic Anion Exchanger Family Member 26A3 (S26A3)	-1.49	-2.84	0.017
	Solute Carrier Organic Anion Transporter Family Member 1A2 (SO1A2)	-1.02	-2.41	0.036
	Solute Carrier Organic Anion Transporter Family Member 2B1 (SO2B1)	1.78	2.38	0.038
Skin	Saxiphilin	2.31	3.14	0.01
	Complement C3	2.72	5.02	0.0005
	Venom Factor	2.58	3.60	0.005
	ATP Binding Cassette Subfamily A Member 5 (ABCA5)	1.55	3.32	0.008
	ATPase Na+/K+ Transporting Subunit Alpha 1 (AT1A1)	-1.14	-2.33	0.042
	Cytochrome P450 2D20 (CP2D20)	-1.92	-3.52	0.006
	Cytochrome P450 2G1 (CP2G1)	2.71	2.96	0.014
	Cytochrome P450 2H2 (CP2H2)	1.54	2.69	0.022
	Cytochrome P450 2K1 (CP2K1)	1.28	3.08	0.012
	Cytochrome P450 2K4 (CP2K4)	-1.89	-3.75	0.004

Table 1. Statistics for protein contigs displayed in Figure 2. The proteins in each tissue are detailed in each row. Results are from the *limma* empirical Bayes analysis and show the log2 fold

change (LogFC) the moderated test statistic (t_{mod}) and the moderated p-value (p_{mod}, adjusted for false discovery rate).

One of the strongest patterns observed in this study was that the complement system, which plays a role in adaptive and innate immunity (Sahu and Lambris, 2001), is more active in toxic frogs (Figure 2A). Specifically, the complement C3 protein (CO3) and a related protein, A.superbus venom factor, were increased in toxic frogs in all tissues (Table 1). Complement C3 has been linked to poison frog toxicity previously through RNA sequencing studies (Caty et al., 2019; Sanchez et al., 2019), but this is the first proteomic evidence across tissues. The significant upregulation of a complement C3-like venom factor was particularly interesting. Venom complement factors were first discovered in cobras and later identified in other venomous animals, like spiders (Tambourgi and van den Berg, 2014). Cobra Venom Factor (CVF)-like proteins are co-injected with toxins from the venom glands, but are not toxic in themselves. Rather, CVF-like proteins activate complement C3 and deplete the complement system in the victim, which increases vascular permeability at the envenomation site, spreading the toxins throughout the prey faster (Vogel and Fritzinger, 2010). Although the function of CVF-like proteins in amphibians is unknown, they could have alkaloid absorption enhancing capabilities, as has been suggested for other amphibian skin peptides (Raaymakers et al., 2017), but further testing is necessary to establish this as a complement-dependent phenomenon.

Across all tissues, a number of membrane proteins that bind small molecules for transport or metabolism were differentially abundant between toxic and control frogs (Figure 2B-D, Table 1). Cytochrome P450s, well known for their small molecule metabolism (Danielson, 2002), were differentially abundant across tissues, with most cytochrome P450s decreasing in abundance with toxicity in the intestines (Figure 2B, S2). This pattern was surprising, as we initially hypothesized that small molecule metabolism capacity would increase with toxin accumulation, and indeed there are some cytochrome P450s that increase with DHQ accumulation in the skin (Figure 2D,

S3). However, this decrease in intestinal cytochrome P450 abundance may instead reflect physiological reduction in metabolism of xenobiotics so that toxins can arrive intact to the skin. Additionally, the abundance of a number of transporter proteins changed with toxin accumulation, including ABC (ATP-binding cassette) transporters (Schinkel and Jonker, 2003) and solute carrier proteins (Lin et al., 2015). These proteins may be important in uptake and transfer of alkaloids across tissues, as both protein families bind to xenobiotics in mammals, including in the context of cancer resistance to alkaloid-based anticancer therapies (Chen et al., 2016; Liu, 2009). Finally, we note that the Na+/K+-ATPase is downregulated with toxin accumulation in the skin. Mutations in this protein have been associated with toxin-resistance mechanisms in many animals (Ujvari et al., 2015) and changing the abundance of this protein may be an additional coping mechanism. More in depth *in vitro* studies with these membrane transporter and metabolism proteins would be required to fully understand these trends and the extent to which these proteins can interact with poison frog alkaloids.

In this study, we show that the Diablito frog can bioaccumulate dietary alkaloids within four days of exposure, and this rapid uptake shifts abundance of proteins that interact with xenobiotics, including plasma carrier proteins, membrane transporters, and cytochrome P450s. Moreover, our study suggests that the complement system and associated venom factors may be involved in alkaloid delivery, although experiments involving frog predators are needed to test this idea. Our study lays a foundation for future work involving rigorous small molecule binding, transport, and metabolism experiments, which are needed to pinpoint specific physiological changes that allow poison frogs to acquire their chemical defenses.

Acknowledgements

We thank Aurora Alvarez-Bullya, Stephanie Caty, and Nora Moskowitz for comments on early versions of this manuscript and Eva Fischer and Alexandre Roland for teaching assistance in the LS50 laboratory course.

Funding

This work was supported a Bauer Fellowship from Harvard University (LAO), the L'Oreal For Women in Science Fellowship (LAO), the National Science Foundation IOS-1557684 (LAO), a Howard Hughes Medical Institute Professor's Award 520008146 (AWM), and the National Institutes of Health R01s GM132129 (JAP) and GM67945 (SPG).

Data Accessibility

Mass spectrometry data are available at PRIDE database (PRoteomics IDEntifications Database) (submission pending). All processed data is in the Supplementary Excel File.

Author Contributions

LAO and AWM designed the research; Harvard College students (LS50:Integrated Science: Marianne T. Aguilar, Sophia M. Caldera, Jacqueline Chea, Miruna G. Cristus, Jett P. Crowdis, Bluyé DeMessie, Caroline R. DesJardins-Park, Audrey H. Effenberger, Felipe Flores, Michael Giles, Emma Y. He, Nike S. Izmaylov, ChangWon C. Lee, Nicholas A. Pagel, Krystal K. Phu, Leah U. Rosen, Danielle A. Seda, Yong Shen, Santiago Vargas, and Hadley S. Weiss) funded by the Howard Hughes Medical Institute Professor's Award 520008146 (AWM) conducted the toxin feeding experiment and preliminary data analyses under the guidance of LAO; JDO and JAP conducted the proteomics experiments; SAT quantified DHQ; SPG and AWM contributed new reagents/tools; LAO analyzed the data and wrote the paper with contributions from all authors.

References

Blighe K, Rana S, Lewis M. 2019. EnhancedVolcano: Publication-ready volcano plots with enhanced colouring and labeling.

Brooks M, Mollie, Brooks E, Kristensen K, Koen, J., Benthem V, Magnusson A, Casper, Berg W, Nielsen A, Hans, Skaug J, Mächler M, Benjamin, Bolker M. 2017. glmmTMB Balances Speed and Flexibility Among Packages for Zero-inflated Generalized Linear Mixed Modeling. *The R Journal*. doi:10.32614/rj-2017-066

Caty SN, Alvarez-Buylla A, Byrd GD, Vidoudez C, Roland AB, Tapia EE, Budnik B, Trauger SA, Coloma LA, O'Connell LA. 2019. Molecular physiology of chemical defenses in a poison frog. *J Exp Biol* **222**. doi:10.1242/jeb.204149

Chen Z, Shi T, Zhang L, Zhu P, Deng M, Huang C, Hu T, Jiang L, Li J. 2016. Mammalian drug efflux transporters of the ATP binding cassette (ABC) family in multidrug resistance: A review of the past decade. *Cancer Lett* **370**:153–164.

Daly JW, Garraffo HM, Spande TF, Clark VC, Ma J, Ziffer H, Cover JF Jr. 2003. Evidence for an enantioselective pumiliotoxin 7-hydroxylase in dendrobatid poison frogs of the genus Dendrobates. *Proc Natl Acad Sci U S A* **100**:11092–11097.

Daly JW, Martin Garraffo H, Spande TF, Jaramillo C, Stanley Rand A. 1994a. Dietary source for skin alkaloids of poison frogs (Dendrobatidae)? *J Chem Ecol* **20**:943–955.

Daly JW, Secunda SI, Garraffo HM, Spande TF, Wisnieski A, Cover JF Jr. 1994b. An uptake system for dietary alkaloids in poison frogs (Dendrobatidae). *Toxicon* **32**:657–663.

Daly JW, Spande TF, Garraffo HM. 2005. Alkaloids from amphibian skin: a tabulation of over eight-hundred compounds. *J Nat Prod* **68**:1556–1575.

D'Angelo G, Chaerkady R, Yu W, Hizal DB, Hess S, Zhao W, Lekstrom K, Guo X, White WI, Roskos L, Bowen MA, Yang H. 2017. Statistical Models for the Analysis of Isobaric Tags Multiplexed Quantitative Proteomics. *J Proteome Res* **16**:3124–3136.

Danielson PB. 2002. The cytochrome P450 superfamily: biochemistry, evolution and drug metabolism in humans. *Curr Drug Metab* **3**:561–597.

Darst CR, Menéndez-Guerrero PA, Coloma LA, Cannatella DC. 2005. Evolution of dietary specialization and chemical defense in poison frogs (Dendrobatidae): a comparative analysis. *Am Nat* **165**:56–69.

Elias JE, Gygi SP. 2010. Target-decoy search strategy for mass spectrometry-based proteomics. *Methods Mol Biol* **604**:55–71.

Hantak MM, Grant T, Reinsch S, Mcginnity D, Loring M, Toyooka N, Saporito RA. 2013. Dietary Alkaloid Sequestration in a Poison Frog: An Experimental Test of Alkaloid Uptake in Melanophryniscus stelzneri (Bufonidae). *J Chem Ecol* **39**:1400–1406.

Huttlin EL, Jedrychowski MP, Elias JE, Goswami T, Rad R, Beausoleil SA, Villén J, Haas W, Sowa ME, Gygi SP. 2010. A tissue-specific atlas of mouse protein phosphorylation and expression. *Cell* **143**:1174–1189.

Lin L, Yee SW, Kim RB, Giacomini KM. 2015. SLC transporters as therapeutic targets: emerging opportunities. *Nat Rev Drug Discov* **14**:543–560.

Liu F-S. 2009. Mechanisms of Chemotherapeutic Drug Resistance in Cancer Therapy—A Quick Review. *Taiwanese Journal of Obstetrics and Gynecology*. doi:10.1016/s1028-4559(09)60296-5

Mahar J, Lukács GL, Li Y, Hall S, Moczydlowski E. 1991. Pharmacological and biochemical properties of saxiphilin, a soluble saxitoxin-binding protein from the bullfrog (Rana catesbeiana). *Toxicon* **29**:53–71.

McAlister GC, Nusinow DP, Jedrychowski MP, Wühr M, Huttlin EL, Erickson BK, Rad R, Haas

W, Gygi SP. 2014. MultiNotch MS3 enables accurate, sensitive, and multiplexed detection of differential expression across cancer cell line proteomes. *Anal Chem* **86**:7150–7158.
McGugan JR, Byrd GD, Roland AB, Caty SN, Kabir N, Tapia EE, Trauger SA, Coloma LA, O'Connell LA. 2016. Ant and Mite Diversity Drives Toxin Variation in the Little Devil Poison Frog. *J Chem Ecol* **42**:537–551.
Neuwirth M, Daly JW, Myers CW, Tice LW. 1979. Morphology of the granular secretory glands in skin of poison-dart frogs (Dendrobatidae). *Tissue Cell* **11**:755–771.
Opitz SEW, Müller C. 2009. Plant chemistry and insect sequestration. *Chemoecology* **19**:117–154.
Prates I, Antoniazzi MM, Sciani JM, Pimenta DC, Toledo LF, Haddad CFB, Jared C. 2011. Skin glands, poison and mimicry in dendrobatid and leptodactylid amphibians. *J Morphol* **273**:279–290.
Raaymakers C, Verbrugghe E, Hernot S, Hellebuyck T, Betti C, Peleman C, Claeys M, Bert W, Caveliers V, Ballet S, Martel A, Pasmans F, Roelants K. 2017. Antimicrobial peptides in frog poisons constitute a molecular toxin delivery system against predators. *Nat Commun* **8**:1495.
Rahnenfuhrer AA. 2019. topGO: Enrichment Analysis for Gene Ontology.
Ritchie ME, Phipson B, Wu D, Hu Y, Law CW, Shi W, Smyth GK. 2015. limma powers differential expression analyses for RNA-sequencing and microarray studies. *Nucleic Acids Res* **43**:e47.
Roland AB, Santos JC, Carriker BC, Caty SN, Tapia EE, Coloma LA, O'Connell LA. 2016. Radiation and hybridization of the Little Devil poison frog (Oophaga sylvatica) in Ecuador. doi:10.1101/072181
Sahu A, Lambris JD. 2001. Structure and biology of complement protein C3, a connecting link between innate and acquired immunity. *Immunol Rev* **180**:35–48.
Sanchez E, Rodríguez A, Grau JH, Lötters S, Künzel S, Saporito RA, Ringler E, Schulz S, Wollenberg Valero KC, Vences M. 2019. Transcriptomic Signatures of Experimental Alkaloid Consumption in a Poison Frog. *Genes* **10**. doi:10.3390/genes10100733
Santos JC, Coloma LA, Cannatella DC. 2003. Multiple, recurring origins of aposematism and diet specialization in poison frogs. *Proc Natl Acad Sci U S A* **100**:12792–12797.
Santos JC, Tarvin RD, O'Connell LA. 2016. A Review of Chemical Defense in Poison Frogs (Dendrobatidae): Ecology, Pharmacokinetics, and AutoresistanceChemical Signals in Vertebrates 13. pp. 305–337.
Saporito RA, Donnelly MA, Spande TF, Martin Garraffo H. 2011. A review of chemical ecology in poison frogs. *Chemoecology* **22**:159–168.
Saporito RA, Spande TF, Martin Garraffo H, Donnelly MA. 2009. Arthropod Alkaloids in Poison Frogs: A Review of the "Dietary Hypothesis." *Heterocycles* **79**:277.
Savitzky AH, Mori A, Hutchinson DA, Saporito RA, Burghardt GM, Lillywhite HB, Meinwald J. 2012. Sequestered defensive toxins in tetrapod vertebrates: principles, patterns, and prospects for future studies. *Chemoecology* **22**:141–158.
Schinkel AH, Jonker JW. 2003. Mammalian drug efflux transporters of the ATP binding cassette (ABC) family: an overview. *Adv Drug Deliv Rev* **55**:3–29.
Stynoski JL, Torres-Mendoza Y, Sasa-Marin M, Saporito RA. 2014. Evidence of maternal provisioning of alkaloid-based chemical defenses in the strawberry poison frog Oophaga pumilio. *Ecology* **95**:587–593.
Tambourgi DV, van den Berg CW. 2014. Animal venoms/toxins and the complement system. *Molecular Immunology*. doi:10.1016/j.molimm.2014.06.020
Ujvari B, Casewell NR, Sunagar K, Arbuckle K, Wüster W, Lo N, O'Meally D, Beckmann C, King GF, Deplazes E, Madsen T. 2015. Widespread convergence in toxin resistance by predictable molecular evolution. *Proc Natl Acad Sci U S A* **112**:11911–11916.
Vogel C-W, Fritzinger DC. 2010. Cobra venom factor: Structure, function, and humanization for

therapeutic complement depletion. *Toxicon* **56**:1198–1222.
Wickham H. 2009. ggplot2: Elegant Graphics for Data Analysis. Springer Science & Business Media.
Yen T-J, Lolicato M, Thomas-Tran R, Du Bois J, Minor DL Jr. 2019. Structure of the saxiphilin:saxitoxin (STX) complex reveals a convergent molecular recognition strategy for paralytic toxins. *Sci Adv* **5**:eaax2650.
Zhang Y, Benet LZ. 2001. The Gut as a Barrier to Drug Absorption. *Clin Pharmacokinet* **40**:159–168.

Supplementary Figures

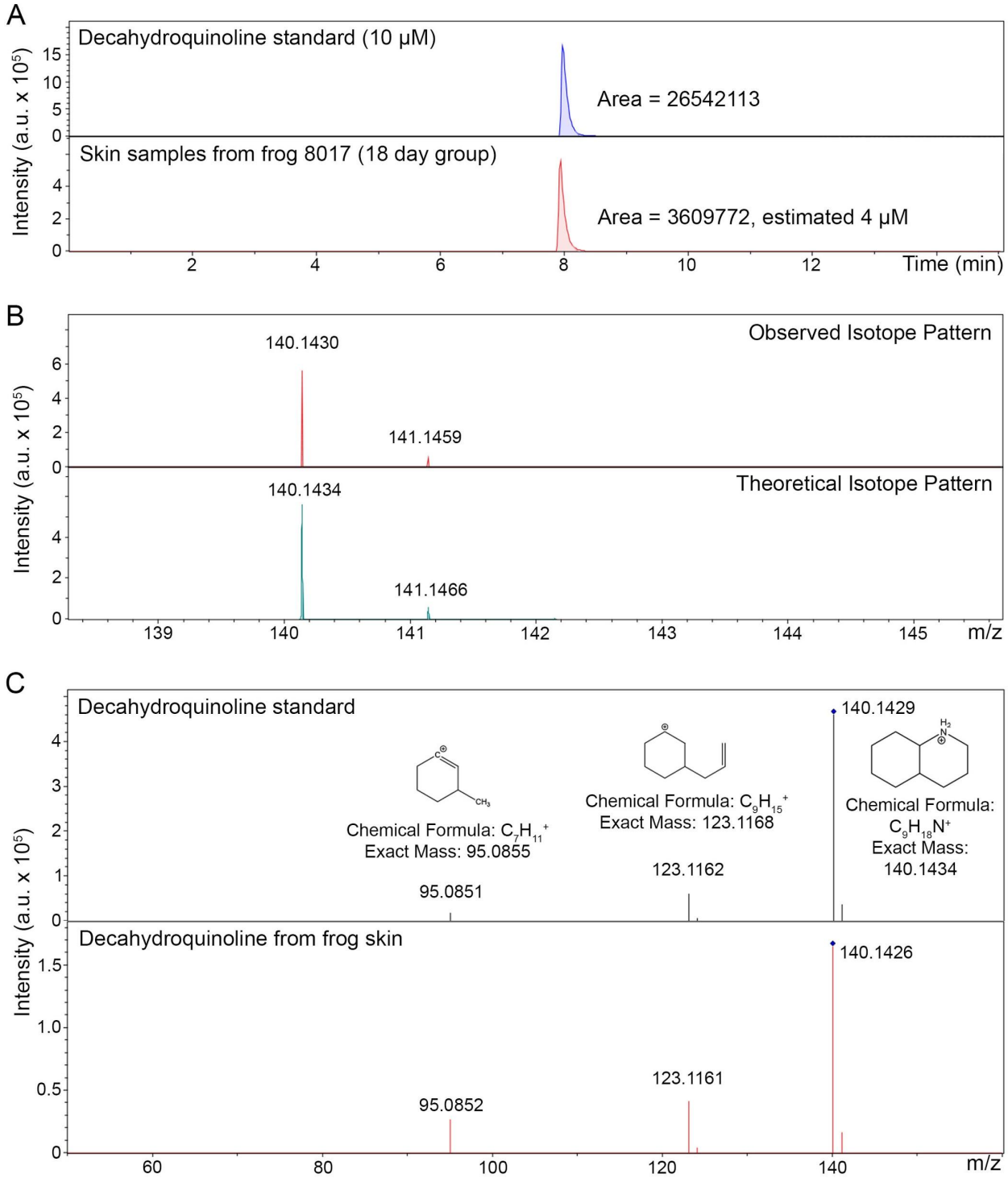

Figure S1. Detection of decahydroquinoline (DHQ) using liquid chromatography / mass spectrometry. (A) DHQ was dissolved at 10μM in methanol and used as a standard (top panel) to quantify tissue samples (bottom panel). **(B)** The observed isotope pattern of the DHQ standard (top panel) matched the theoretical expectation (bottom panel). **(C)** Tandem mass spectrometry was used to confirm the structure of DHQ from frog skin with the standard.

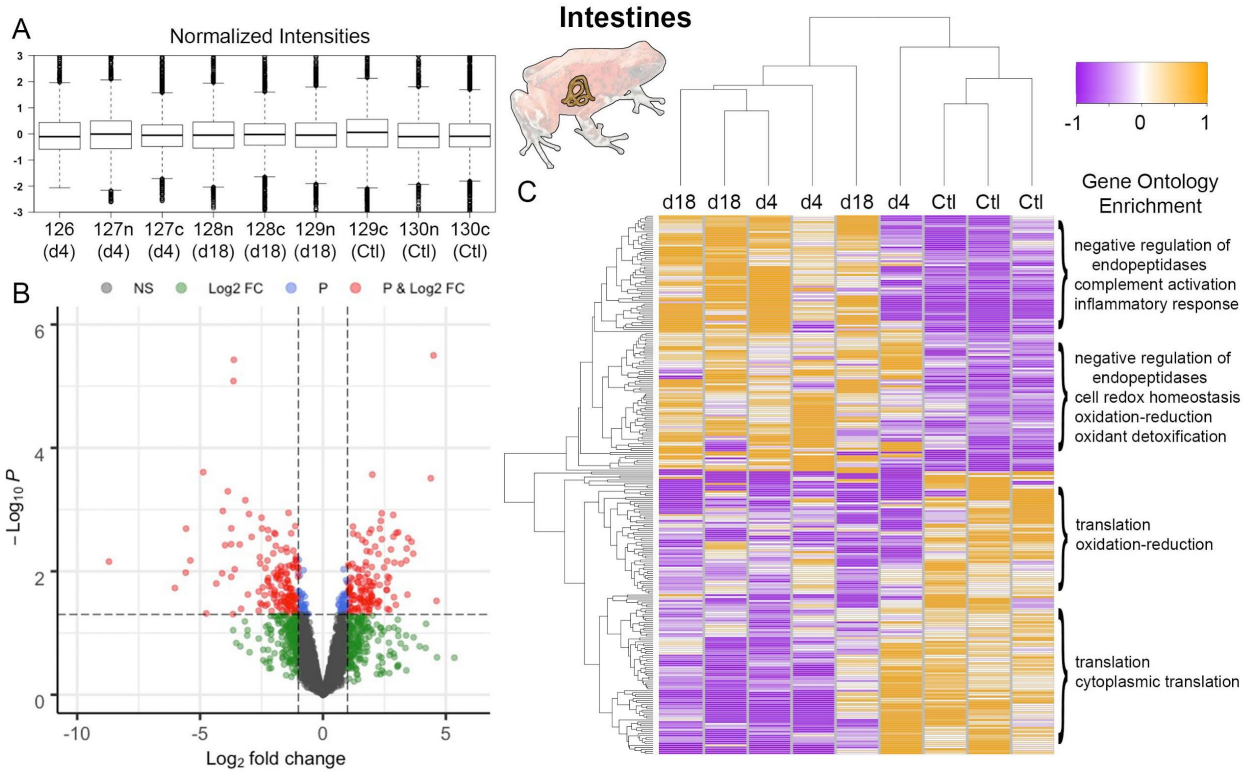

Figure S2. Quantification of protein changes in the intestines with decahydroquinoline bioaccumulation. (A) Protein samples were tandem mass tag (TMT) labeled prior to quantification and channels were z-score normalized prior to analysis. **(B)** Volcano plots show protein contigs that are not significant (NS, black), log fold change greater than one (Log2 FC, green), a p-value < 0.05 (P, blue) or both (red). **(C)** Heatmap of protein contig abundance (rows) between individuals frogs (columns); gene ontology enrichments in different clusters are on the right.

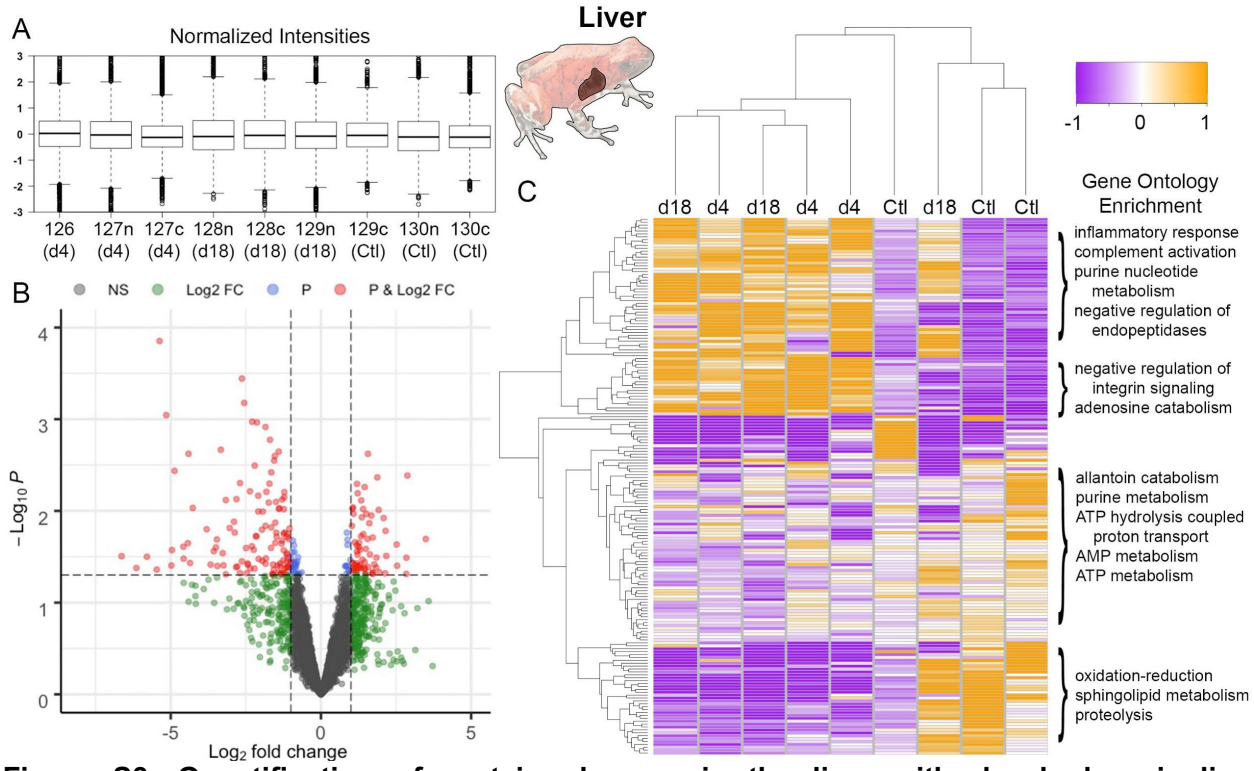

Figure S3. Quantification of protein changes in the liver with decahydroquinoline bioaccumulation. (A) Protein samples were tandem mass tag (TMT) labeled prior to quantification and channels were z-score normalized prior to analysis. **(B)** A volcano plot shows protein contigs that are not significant (NS, black), log fold change greater than one (Log2 FC, green), a p-value < 0.05 (P, blue) or both (red). **(C)** A heatmap of protein contig abundance (rows) between individuals frogs (columns); gene ontology enrichments in different clusters are on the right.

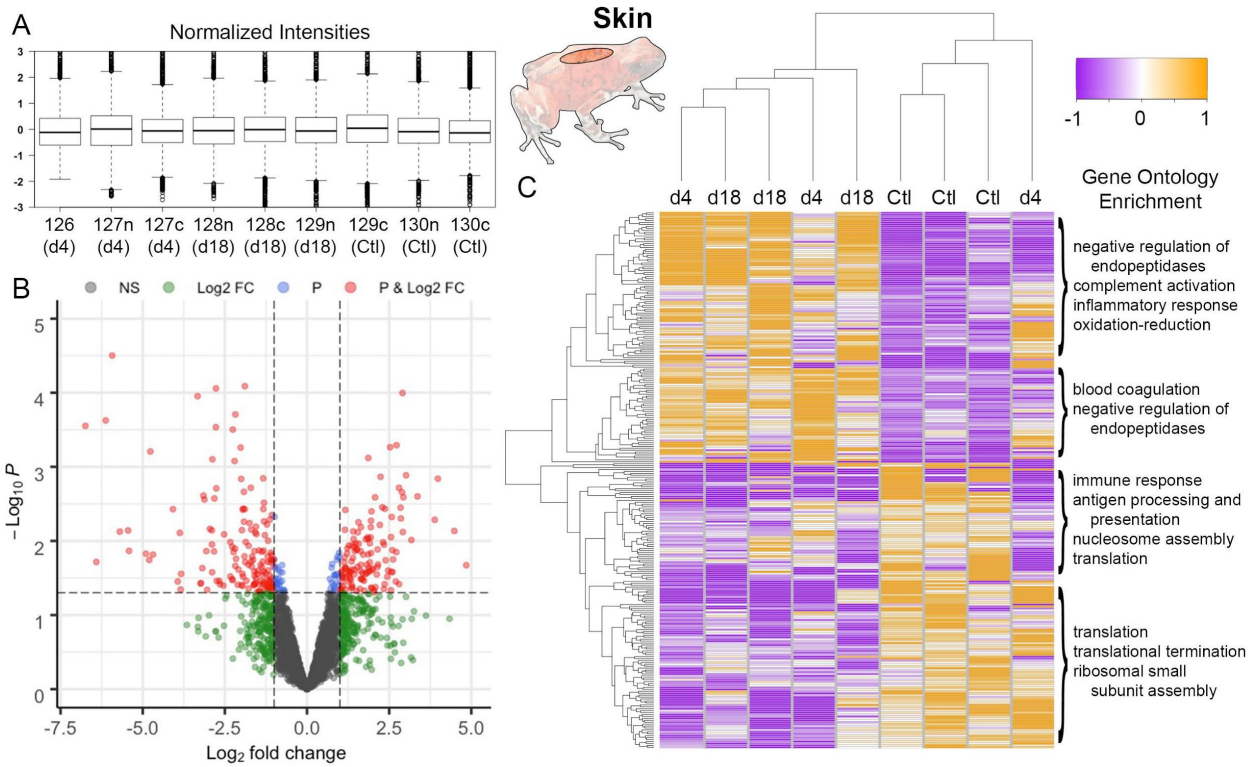

Figure S4. Quantification of protein changes in the skin with decahydroquinoline bioaccumulation. (A) Protein samples were tandem mass tag (TMT) labeled prior to quantification using mass spectrometry. Channels were z-score normalized prior to analysis. **(B)** A volcano plot shows protein contigs that are not significant (NS, black), log fold change greater than one (Log2 FC, green), a p-value < 0.05 (P, blue) or both (red). **(C)** A heatmap of protein contig abundance (rows) between individuals frogs (columns); gene ontology enrichments in different clusters are on the right.